IEEE Access
Multidisciplinary ⋮ Rapid Review ⋮ Open Access Journal

Received January 6, 2021, accepted January 14, 2021, date of publication January 21, 2021, date of current version February 2, 2021.

*Digital Object Identifier 10.1109/ACCESS.2021.3053395*

# An Improved Dynamic Model Updating Method for Multistage Gearbox Based on Surrogate Model and Sensitivity Analysis

**HUACHAO XU[1], DATONG QIN[1], CHANGZHAO LIU[1], AND YANG ZHANG[2]**
[1]State Key Laboratory of Mechanical Transmissions, Chongqing University, Chongqing 400030, China
[2]School of Mechanical Engineering, Dalian University of Technology, Dalian 116024, China

Corresponding author: Huachao Xu (xuhuachao@cqu.edu.cn)

This work was supported by the National Natural Science Foundation of China under Grant 51705042.

**ABSTRACT** Model updating can improve the accuracy of the multistage gearbox dynamic model (MGDM). However, owing to the time-consuming calculations and numerous parameters of the MGDM, previous updating methods are not suitable for updating the MGDM. To solve the above problems, an improved dynamic model updating method that is suitable for updating the MGDM is proposed in this paper. Compared with previous methods, this updating method presents two improvements: (1) In the iterative calculation process, the surrogate model is used to replace the time-consuming MGDM, thereby solving the problem of low computational efficiency; (2) before the updating calculation, Sobol sensitivity analysis is performed to screen out updating parameters from numerous parameters. This study shows that the accuracy of the updated MGDM improved significantly compared with the initial model, thereby enabling a more accurate prediction of the dynamic characteristics of the actual system. This proves the effectiveness of the improved updating method.

**INDEX TERMS** Gear, gearbox, dynamic model, updating method, sensitivity analysis, surrogate model.

## I. INTRODUCTION

Multistage gearboxes are widely used in vehicles, aviation, aerospace, marine, and other fields [1]–[3]. In dynamic design, the establishment of a multistage gearbox dynamic model (MGDM) that can reflect the dynamic characteristics of the actual system is the basis for response prediction, system optimization, and vibration evaluation. However, owing to the complexity of the multistage gearbox as well as simplifications and assumptions made in modeling, it is difficult for the initial MGDM to reflect the dynamic characteristics of the actual system. Therefore, it is necessary to update the initial MGDM based on experimental results to improve the accuracy of the calculation results.

The model updating is based on the experimental results, and the error between simulation and experimental results is minimized by adjusting the matrix or parameters appropriately to improve the model accuracy [4]. Currently, model updating methods are primarily categorized into direct updating and iterative updating [5]. The updating object of the direct updating method is typically the model matrix, i.e., the model can be updated directly by adjusting the mass, stiffness, or damping matrix of the model. Although this method can improve the model accuracy, it is difficult to determine the physical sense of the updated model matrix. The updating object of the iterative updating method is generally the model parameters. This method not only affords a good updating effect but also retains the original physical sense after the updated parameters are determined. However, the iterative updating method typically requires a large amount of iterative calculations to complete the model updating. When the previous iterative updating method is directly used to update the MGDM, its updating efficiency is extremely low. However, the development of surrogate models can solve the low updating efficiency problem of the MGDM [6]–[9].

The essence of the iterative updating method is to apply the optimization algorithm to find the optimal parameters within the value range of the updating parameters such that the simulation results are closest to the experimental results [10]. However, when many updating parameters are involved,

The associate editor coordinating the review of this manuscript and approving it for publication was Agustin Leobardo Herrera-May.

the previous iterative updating method is directly used to update the MGDM; this not only results in an extremely low computational efficiency but also renders it easy for the updating target to fall into a local optimum [11]. Therefore, the screening of both updating and sensitive parameters are critical for MGDM updating. Sensitivity analysis can evaluate the effect of each parameter on the system output and is an effective method to screen the updating parameters. The Sobol method is a sensitivity analysis method based on variance [12] that can effectively determine the sensitive parameters and provide an important basis for the screening of updating parameters for the MGDM.

In summary, improving the calculation efficiency and screening the updating parameters are important prerequisites and key issues in updating the MGDM. However, the previous updating methods have failed to solve these problems; therefore, it is difficult to update the MGDM. Hence, based on a surrogate model and sensitivity analysis, an improved dynamic model iterative updating method is proposed herein. First, the MGDM was established using the lumped parameter/finite element method. Subsequently, kriging (KRG), a radial basis function (RBF), and a support vector machine (SVM) were used to construct surrogate models of the MGDM. KRG was selected as the final surrogate model for the subsequent Sobol sensitivity analysis and genetic updating through accuracy comparison. Next, Sobol sensitivity analysis was performed to screen the updating parameters of the MGDM. Finally, the genetic algorithm was used to determine the most suitable parameters within the value range of the updating parameters to minimize the errors between simulation and experimental results. The remainder of this paper is organized as follows: In Section 2, the surrogate model and Sobol sensitivity analysis theory are introduced. Section 3 presents the use of the lumped parameter/finite element method to establish the MGDM. The update of the MGDM using the proposed updating method is presented in Section 4. Finally, the conclusion is presented in Section 5.

## II. THEORY

This section introduces the surrogate model and Sobol sensitivity analysis theory employed in this study.

### A. SURROGATE MODEL

The surrogate model can accurately reflect the relationship between the input and output of the MGDM, thereby effectively replacing the MGDM. Compared with the MGDM, the surrogate model requires less computation, and its prediction accuracy satisfies the analysis requirements. Therefore, the surrogate model was adopted in this study, replacing the time-consuming MGDM, to solve the problem of low computational efficiency.

Currently, surrogate models suitable for the MGDM with high-dimensional input include KRG, the RBF, and the SVM. This section introduces the theory of these surrogate models.

#### 1) KRG

KRG is an unbiased estimation model with minimum estimation variance that has been widely used in engineering because of its good fitting ability [13], [14]. The predicted value y(x) of KRG comprises a regression part and a non-parametric part. It is expressed as

$$y(\boldsymbol{x}) = \sum_{j=1}^{k} \beta_j f_j(\boldsymbol{x}) + z(\boldsymbol{x}), \tag{1}$$

where $\boldsymbol{x}$ represents the training sample; $\beta_j$ represents the regression parameters; $f_j(\boldsymbol{x})$ represents the polynomial function of the training sample; and $z(\boldsymbol{x})$ represents the random error, and its covariance is expressed as [13], [14]

$$cov\left[z(\boldsymbol{x}_i), z(\boldsymbol{x}_j)\right] = \sigma^2 \sum_{n=1}^{N} R_n(d_n), \tag{2}$$

where $N$ represents the number of input variables.

$d_n = \left|x_n^i - x_n^j\right|$ the distance between sample points $x_i$ and $x_j$ in the $n$th variable, and $\sigma^2$ the variance of $z(\boldsymbol{x})$.

#### 2) RBF

RBF is used to fit multivariate functions using discrete data [15]–[17]. Typically, RBF is used as a Gaussian function, expressed as follows:

$$R(\boldsymbol{x}_i - c_p) = \exp(-\frac{1}{2\sigma^2}\left\|x_i - c_p\right\|^2), \tag{3}$$

where $\boldsymbol{x}_i (i = 1, 2, \ldots, l)$ represents the training sample, $l$ represents the sample number, $c_p$ represents the center value of the Gaussian function, and $\sigma$ represents the variance of the Gaussian function.

Finally, the output of RBF is constructed via linear superposition, as follows:

$$y_j = \sum_{i=1}^{h} \omega_{ij} \exp(-\frac{1}{2\sigma^2}\left\|x_p - c_p\right\|^2), \tag{4}$$

where $\omega_{ij} (i = 1, 2, \ldots, h; j = 1, 2, \ldots, t)$ represents the connection weight between the hidden layer node $i$ and output layer node $j$, $h$ represents the node number of the hidden layer, $t$ represents the node number of the output layer, and $y_j$ represents the predicted value of output layer node $j$.

#### 3) SVM

SVM can establish a regression function between the input and output of the original model to replace the original model [18]–[20]. The expression of the mapping relationship between model input $\boldsymbol{x}$ and output $f(\boldsymbol{x})$ is as follows:

$$f(\boldsymbol{x}) = \boldsymbol{w} \cdot \phi(\boldsymbol{x}) + b, \tag{5}$$

where $\phi(\boldsymbol{x})$ represents the mapping function. $\boldsymbol{w}$ and $b$ are the parameters to be calculated, which can be obtained using the

following optimization model [18]–[20]:

$$\begin{cases} \min R(\boldsymbol{w}, \xi, \xi^*, \varepsilon) = \frac{1}{2}\|\boldsymbol{w}\|^2 + C(\nu\varepsilon + \frac{1}{l}\sum_{i=1}^{l}(\xi + \xi^*)) \\ \text{s.t.} \begin{cases} y_i - \boldsymbol{w}\phi(\boldsymbol{x}_i) - b \le \varepsilon + \xi_i & i = 1, 2, \cdots, l \\ \boldsymbol{w}\phi(\boldsymbol{x}_i) + b - y_i \le \varepsilon + \xi_i \\ \xi_i^*, \qquad\qquad\qquad\qquad \varepsilon \ge 0, \end{cases} \end{cases} \tag{6}$$

where $\xi$ and $\xi^*$ represent slack variables, $\varepsilon$ represents the training error, $C$ represents the penalty factor, and $l$ represents the total number of samples.

By introducing the Lagrangian function, Eq. (6) can be rewritten to calculate the form of the Lagrangian operators $\alpha_i$ and $\alpha_i^*$, namely

$$\begin{cases} \max R(\alpha_i, \alpha_i^*) = \sum_{i=1}^{l} y_i(\alpha_i^* - \alpha_i) \\ \qquad\qquad - \frac{1}{2}\sum_{i,j=1}^{l}(\alpha_i - \alpha_i^*)(\alpha_j - \alpha_j^*)K(\boldsymbol{x}_i, \boldsymbol{x}_j) \\ \text{s.t.} \begin{cases} \sum_{i=1}^{l}(\alpha_i - \alpha_i^*) = 0 \\ 0 \le \alpha_i, \alpha_i^* \le C/l \\ \sum_{i=1}^{l}(\alpha_i + \alpha_i^*) \le C \cdot v, \end{cases} \end{cases} \tag{7}$$

where $K(\boldsymbol{x}_i, \boldsymbol{x}_j)$ represents the kernel function, expressed as follows:

$$K(\boldsymbol{x}_i, \boldsymbol{x}_j) = \exp(-\gamma \left\|\boldsymbol{x}_i - \boldsymbol{x}_j\right\|^2), \gamma \ge 0, \tag{8}$$

where $\gamma$ represents the nuclear parameters.

The expression to calculate the predicted value is

$$f(\boldsymbol{x}) = \sum_{i=1}^{l}(\alpha_i^* - \alpha_i)K(\boldsymbol{x}_i, \boldsymbol{x}_j) + b. \tag{9}$$

### B. SOBOL SENSITIVITY ANALYSIS

The Sobol method is a quantitative sensitivity analysis method based on variance that can quantitatively evaluate the effect of each input variable on the system output [21]. The Sobol method was used in this study to analyze the parameter sensitivity of the MGDM to screen the updating parameters. This section introduces the theory of the Sobol method.

It is assumed that the analytical model can be decomposed into a sum of $2^k$ terms, expressed as follows:

$$Y = f_0 + \sum_{i=1}^{k} f_i(x_i) + \sum_{i<j}^{k} f_{ij}(x_i, x_j) + \cdots + f_{i,2,\cdots,k}(x_1, x_2, \cdots, x_k), \tag{10}$$

where

$$\begin{cases} f_0 = E(Y) \\ f_i(x_i) = E(Y/x_i) - f_0 \\ f_{ij}(x_i, x_j) = E(Y/x_i, x_j) - f_0 - f_j, \end{cases} \tag{11}$$

where $f_0$ represents a constant, $f_i$ represents the effect of variable $x_i$ on the system output, and $f_{ij}$ represents the effect of the combined action of variables $x_i$ and $x_j$ on the system output.

If the variables are independent of each other, then each term on the right side of Eq. (10) is orthogonal to each other, and the covariance is zero. Therefore, the expression of Eq. (10) after calculating the variance is as follows:

$$V(Y) = \sum_{i=1}^{k} V_i(x_i) + \sum_{i<j}^{k} V_{ij}(x_i, x_j) + \cdots + V_{i,2,\cdots,k}(x_1, x_2, \cdots, x_k) \tag{12}$$

Among them,

$$\begin{cases} V_i = \mathrm{Var}_{x_i}(Ex_{\sim i}(Y|x_i)) \\ V_{ij} = \mathrm{Var}_{x_{ij}}(Ex_{\sim ij}(Y|x_i, x_j)) - V_i - V_j, \end{cases} \tag{13}$$

where $V(Y)$ represents the total variance, $V_i$ represents the variance of variable $x_i$ to the system output, and $V_{ij}$ represents the variance of the system output due to the simultaneous action of variables $x_i$ and $x_j$.

The local sensitivity $S_i$ represents the effect of individual variable $x_i$ on the system output, calculated as follows:

$$S_i = \frac{V_i}{V(Y)} \tag{14}$$

The global sensitivity $S_{Ti}$ represents the effect of the simultaneous action of variable $x_i$ and other variables on the system output, calculated as

$$S_{\mathrm{T}i} = 1 - \frac{V_{\sim i}}{V(Y),} \tag{15}$$

where $V_{\sim i}$ represents the variance produced by parameters other than variable $x_i$.

## III. MGDM

In this study, the MGDM was established by using the lumped parameter/finite element method, which considers the structural flexibility of the shaft and housing as well as internal excitations such as time-varying meshing stiffness.

### A. GEAR LUMPED PARAMETER MODEL

#### 1) PLANETARY GEAR MODEL

Fig. 1 shows the lumped parameter model of a planetary gear. To facilitate the coupling between the ring and housing, the ring was assumed to be rigid in this study. $\mathrm{p}_n (n = 1, 2, \ldots, N)$, r, c, and s denote planet $n$, ring, carrier, and sun respectively; $N$ denotes the planet number. $k_{\mathrm{rt}}$, $k_{\mathrm{r}}$, and $k_{\mathrm{p}_n}$ denote the ring torsional stiffness, and the radial support stiffness of the ring and planet $n$, respectively. $c_{\mathrm{rt}}$, $c_{\mathrm{r}}$, and $c_{\mathrm{p}_n}$ denote the ring torsional damping, and the radial support damping of the ring and planet $n$, respectively. $e_m$ represents the mesh error. $x_i$, $y_i$, and $\theta_i$ ($i = \mathrm{s}, \mathrm{r}, \mathrm{c}$) represent the radial displacement and angular displacement of the central member. $\eta_{\mathrm{p}_n}$ and $\xi_{\mathrm{p}_n}$ represent the tangential and radial displacements of planet $n$. $\theta_{\mathrm{p}_n}$ represents the angular displacement of planet $n$.

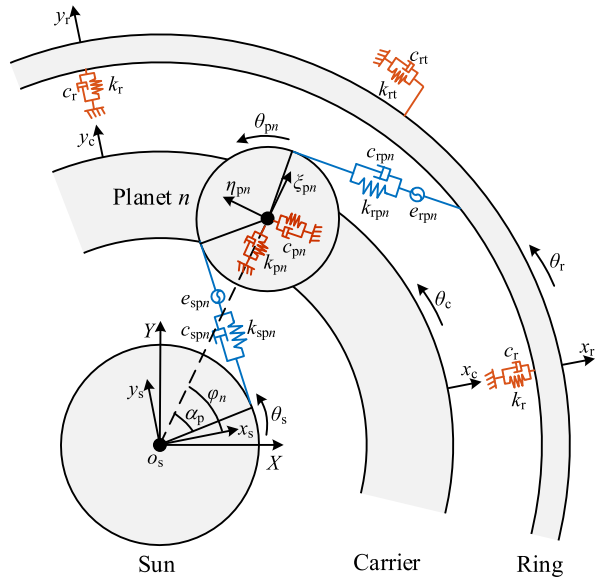


**FIGURE 1.** Lumped parameter model of planetary gear.

The time-varying mesh stiffness $k_m(t)$ ($m = \mathrm{rp}n, \mathrm{sp}n$) of the gear pair can be expressed as

$$k_m(t) = \bar{k}_m + \sum_{i=1}^{10} a_i \cos(l f_m t + \gamma_m), \tag{16}$$

where $\bar{k}_m$ denotes the average mesh stiffness, $a_i$ denotes the Fourier series expansion coefficient, $l$ denotes the harmonic order, $f_\mathrm{m}$ denotes the mesh frequency, and $\gamma_\mathrm{m}$ denotes the mesh phase.

The expression to calculate mesh damping is [22]

$$c_\mathrm{m} = 2\varsigma_\mathrm{m}\sqrt{\bar{k}_m m_\mathrm{p} m_i/(m_\mathrm{p} + m_i)}, \tag{17}$$

where $\varsigma_\mathrm{m}$ denotes the mesh damping ratio, and $m_i$ denotes the mass.

The projection vectors of the internal and external gear pairs along the mesh line direction are as follows: [23]

$$\begin{cases} V_{\mathrm{sp}n} = [\sin\phi, -\cos\phi, -r_\mathrm{bs}, -\sin\alpha_\mathrm{p}, \cos\alpha_\mathrm{p}, -r_\mathrm{bp}] \\ V_{\mathrm{rp}n} = [\sin\alpha_\mathrm{p}, \cos\alpha_\mathrm{p}, r_\mathrm{bp}, -\sin\phi, -\cos\phi, -r_\mathrm{br}], \end{cases} \tag{18}$$

where $r_{\mathrm{b}_k}(k = \mathrm{s}, \mathrm{p}, \mathrm{r})$ denotes the base circle radius, $\phi$ denotes the angle between the $X$-axis and mesh line direction, and $\alpha_\mathrm{p}$ denotes the mesh angle.

Hence, the mass matrix $\boldsymbol{M}_m$, stiffness matrix $\boldsymbol{K}_m$, damping matrix $\boldsymbol{C}_m$, and excitation vector $\boldsymbol{F}_m$ of the internal and external gear pairs can be obtained as follows:

$$\begin{cases} \boldsymbol{K}_m(t) = k_m(t)\boldsymbol{V}_m^T\boldsymbol{V}_m \\ \boldsymbol{C}_m = c_m\boldsymbol{V}_m^T\boldsymbol{V}_m \\ \boldsymbol{F}_m(t) = [k_m(t)e_m(t) + c_m\dot{\boldsymbol{e}}_m(t)]\boldsymbol{V}_m^\mathrm{T} \\ \boldsymbol{M}_m = diag[m_i, m_i, I_i, m_\mathrm{p}, m_\mathrm{p}, I_\mathrm{p}], \end{cases} \tag{19}$$

where $I_i$ denotes the moment of inertia; $\boldsymbol{e}_m(t)$ and $\dot{\boldsymbol{e}}_m(\mathrm{t})$ denote the equivalent displacement and velocity vectors of the mesh error, respectively.

### 2) HELICAL GEAR MODEL

Fig. 2 shows the lumped parameter model of a helical gear pair, where subscripts 5 and 6 denote the driving and driven gears, respectively. $r_{\mathrm{b}_j}(j = 5, 6)$ denotes the base circle radius; $\theta_{j_\mathrm{x}}$ denotes the angular displacement; $\theta_{j_\mathrm{y}}$ and $\theta_{j_\mathrm{z}}$ denote the gear swing angles; $k_{56}$, $c_{56}$, and $\alpha_{56}$ denote the time-varying mesh stiffness, mesh damping, and mesh angle, respectively; and $\phi_{56}$ denotes the shaft position angle.

The dynamic transmission error of a helical gear pair along the mesh line direction is expressed as

$$\delta_{56}(t) = \boldsymbol{V}_{56}\boldsymbol{q}_{56} - e_{56}(t), \tag{20}$$

where $\boldsymbol{q}_{56}$ denotes the displacement vector; $e_{56}$ denotes the mesh error; and $\boldsymbol{V}_{56}$ denotes the projection vector of the helical gear pair along the mesh line direction, expressed as [24]

$$\begin{aligned} \boldsymbol{V}_{56} = [&\cos\beta\sin\varphi, \varepsilon\sin\beta, \varepsilon\cos\beta\cos\varphi, \\ &-\varepsilon r_{b5}\sin\beta\sin\varphi, \varepsilon r_{b5}\cos\beta, -\varepsilon r_{b5}\sin\beta\cos\varphi, \\ &-\cos\beta\sin\varphi, -\varepsilon\sin\beta, -\varepsilon\cos\beta\cos\varphi, \\ &-\varepsilon r_{b6}\sin\beta\sin\varphi, \varepsilon r_{b6}\cos\beta, -\varepsilon r_{b6}\sin\beta\cos\varphi], \end{aligned} \tag{21}$$

where $\beta$ denotes the base circle helix angle; $\varepsilon$ denotes the sign function; and $\varphi$ denotes the angle between the mesh plane and the y-axis, where $\varphi = \alpha_{56} + \varepsilon\phi_{56}$.

Hence, the mass matrix $\boldsymbol{M}_{56}$, stiffness matrix $\boldsymbol{K}_{56}$, damping matrix $\boldsymbol{C}_{56}$, and excitation vector $\boldsymbol{F}_{56}$ of the helical gear pair can be obtained as follows:

$$\begin{cases} \boldsymbol{K}_{56}(t) = k_{56}(t)\boldsymbol{V}_{56}^T\boldsymbol{V}_{56} \\ \boldsymbol{C}_{56} = c_{56}\boldsymbol{V}_{56}^T\boldsymbol{V}_{56} \\ \boldsymbol{F}_{56}(t) = [k_{56}(t)e_{56}(t) + c_{56}\dot{e}_{56}(t)]\,\boldsymbol{V}_{56}^T \\ \boldsymbol{M}_{56} = diag[m_5, m_5, m_5, I_{5x}, I_{5y}, I_{5z}, \\ \qquad m_6, m_6, m_6, I_{6x}, I_{6y}, I_{6z}] \end{cases} \tag{22}$$

### 3) SPIRAL BEVEL GEAR MODEL

Fig. 3 shows the lumped parameter model of a spiral bevel gear pair, where subscripts p and g denote the driving and driven gears, respectively. $\theta_\mathrm{p}$ and $\theta_\mathrm{g}$ denote the gear angular displacements; $\delta_\mathrm{n}$, $\beta_\mathrm{n}$, and $\alpha_\mathrm{n}$ denote the pitch cone angle, and the midpoint helix angle and pressure angle of the driving gear, respectively; $k_\mathrm{n}$, $c_\mathrm{n}$, and $e_\mathrm{n}$ denote the time-varying mesh stiffness, mesh damping, and mesh error, respectively.

The dynamic transmission error of a spiral bevel gear pair along the mesh line direction is

$$\delta_{\mathrm{pg}}(t) = \boldsymbol{V}_\mathrm{n}\boldsymbol{q}_\mathrm{n} - e_\mathrm{n}(t), \tag{23}$$

where $\boldsymbol{q}_\mathrm{n}$ denotes the displacement vector; $\boldsymbol{V}_\mathrm{n}$ denotes the projection vector of the spiral bevel gear pair along the mesh line direction. Based on the force analysis in Fig. 4, $\boldsymbol{V}_\mathrm{n}$ can be expressed as follows [25]:

$$\boldsymbol{V}_\mathrm{n} = [(\sin\alpha_\mathrm{n}\cos\delta_\mathrm{n} + \cos\alpha_\mathrm{n}\sin\beta_\mathrm{n}\sin\delta_\mathrm{n}),$$

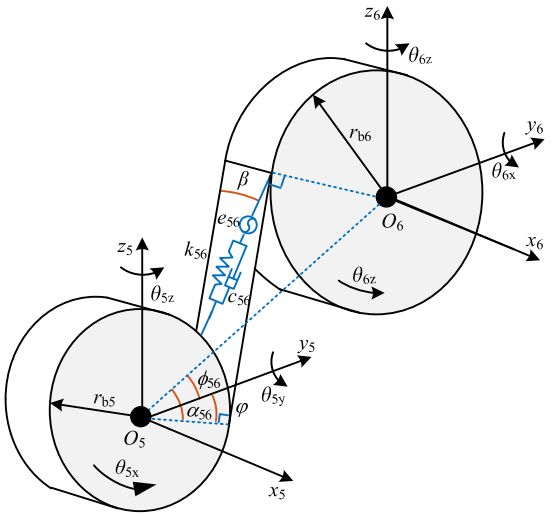


**FIGURE 2.** Lumped parameter model of helical gear pair.

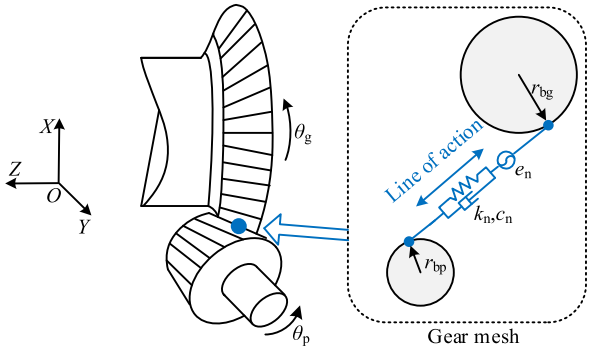


**FIGURE 3.** Lumped parameter model of spiral bevel gear pair.

$$
\begin{aligned}
&-(\sin\alpha_n \sin\delta_n - \cos\alpha_n \sin\beta_n \cos\delta_n),\\
&\cos\alpha_n \cos\beta_n, r_{bp}\cos\alpha_n \sin\beta_n,\\
&-(\sin\alpha_n \cos\delta_n + \cos\alpha_n \sin\beta_n \sin\delta_n),\\
&(\sin\alpha_n \sin\delta_n - \cos\alpha_n \sin\beta_n \cos\delta_n),\\
&-\cos\alpha_n \cos\beta_n, -r_{bg}\cos\alpha_n \sin\beta_n],
\end{aligned} \tag{24}
$$

Hence, the mass matrix $\boldsymbol{M}_{pg}$, stiffness matrix $\boldsymbol{K}_{pg}$, damping matrix $\boldsymbol{C}_{pg}$, and excitation vector $\boldsymbol{F}_{pg}$ of the spiral bevel gear pair can be obtained as follows:

$$
\begin{cases}
\boldsymbol{K}_{pg}(t) = k_n(t)\boldsymbol{V}_n^T\boldsymbol{V}_n\\
\boldsymbol{C}_{pg} = c_n\boldsymbol{V}_n^T\boldsymbol{V}_n\\
\boldsymbol{M}_{pg} = diag[m_p, m_p, m_p, I_p, m_g, m_g, m_g, I_g]\\
\boldsymbol{F}_{pg}(t) = [k_n(t)e_n(t) + c_n\dot{e}_n(t)]\boldsymbol{V}_n^T
\end{cases} \tag{25}
$$

### B. FINITE ELEMENT MODEL OF SHAFT AND HOUSING

To consider structural flexibility, a shaft finite element model was constructed using Beam188 elements in the finite element simulation platform, as shown in Fig. 5. Subsequently, the reduction method was used to reduce the degrees of freedom of the shaft finite element model, and a condensed finite element model of the shaft was obtained.

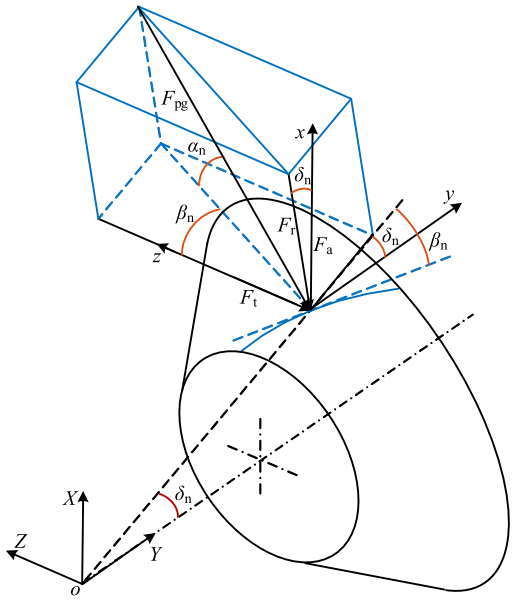


**FIGURE 4.** Force analysis of spiral bevel gear.

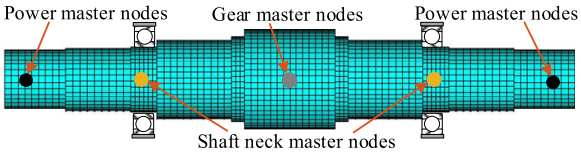


**FIGURE 5.** Finite element model of transmission shaft.

Furthermore, a housing finite element model was established based on the finite element simulation platform (see Fig. 6). The material used was aluminum alloy, whose density, elastic modulus, and Poisson's ratio were $2.7 \times 10^3$ kg/m$^3$, $7.1 \times 10^{10}$ N/m$^2$, and 0.33, respectively. The Solid92 solid element was used to mesh the housing structure. The model comprised 569028 elements and 969948 nodes. Subsequently, the degrees of freedom of the housing finite element model were reduced using the reduction method, and the condensed finite element model of housing was obtained.

### C. BEARING MODEL

In the system model, the transmission shaft was coupled with the housing through the bearing. The stiffness matrix $\boldsymbol{K}_b$ of the bearing is expressed as [23]

$$
\boldsymbol{K}_b = diag[k_x, k_y, k_z, k_{\theta x}, k_{\theta y}, 0], \tag{26}
$$

where $k_x$, $k_y$, and $k_z$ represent the support stiffness along the generalized coordinate axis direction; $k_{\theta x}$ and $k_{\theta y}$ represent the swing stiffness of the bearing.

The bearing damping is calculated as follows:

$$
\boldsymbol{C}_b = \zeta_b\boldsymbol{K}_b, \tag{27}
$$

where $\zeta_{bk}$ represents the bearing damping ratio.

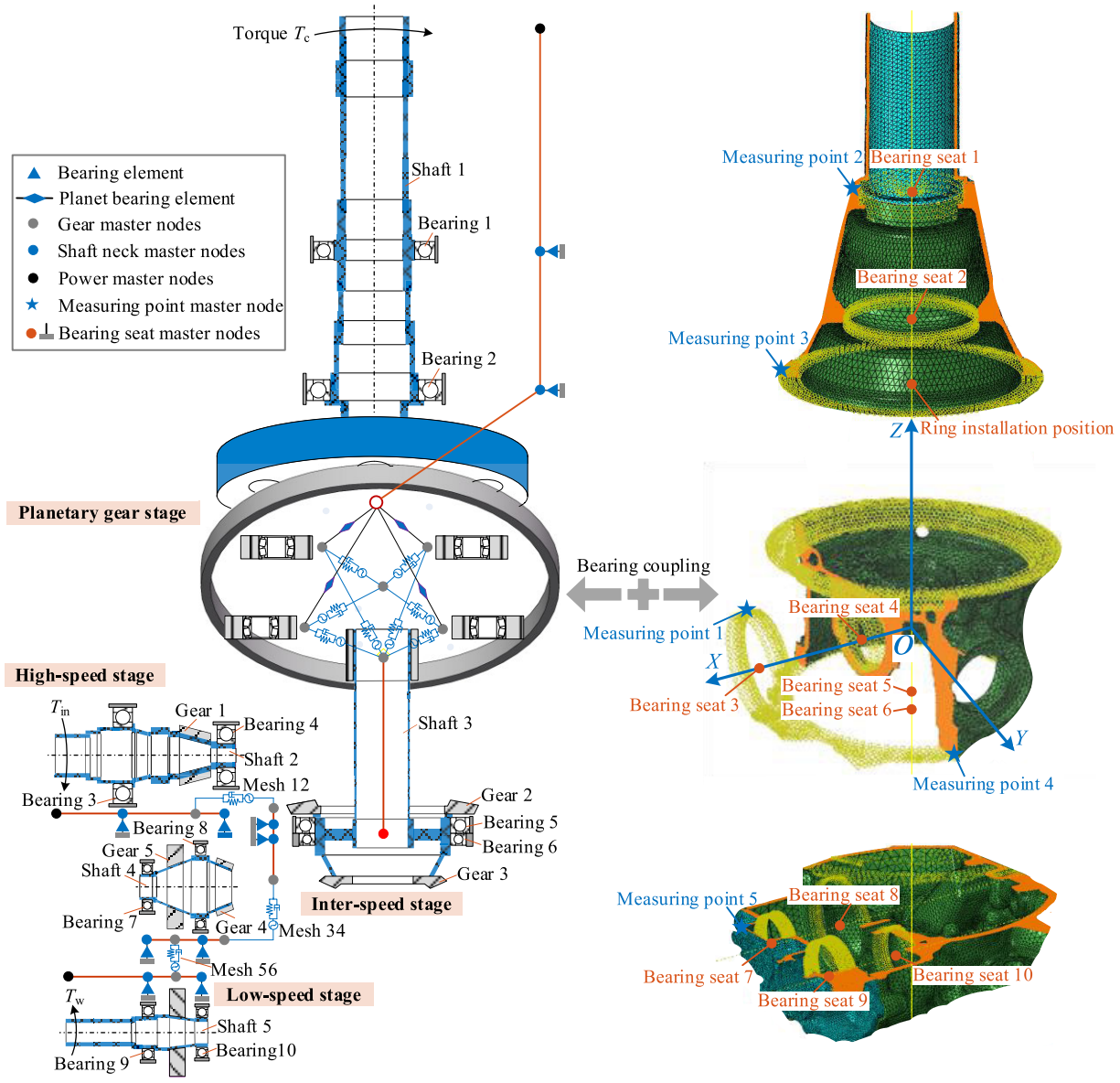


**FIGURE 6.** MGDM.

### D. SYSTEM DYNAMICS MODEL

The coupling relationship between the transmission system and flexible housing is shown in Eq. (28). The shaft neck main node $\boldsymbol{q}_{\mathrm{n}}$ and housing bearing seat main node $\boldsymbol{q}_{\mathrm{h}}$ were coupled via the bearing stiffness matrix $\boldsymbol{K}_{\mathrm{b}}$.

$$\begin{bmatrix} \boldsymbol{M}_n & 0 \\ 0 & \boldsymbol{M}_h \end{bmatrix} \begin{bmatrix} \ddot{\boldsymbol{q}}_n \\ \ddot{\boldsymbol{q}}_h \end{bmatrix} + \begin{bmatrix} \boldsymbol{C}_n + \boldsymbol{C}_b & -\boldsymbol{C}_b \\ -\boldsymbol{C}_b & \boldsymbol{C}_h + \boldsymbol{C}_b \end{bmatrix} \begin{bmatrix} \dot{\boldsymbol{q}}_n \\ \dot{\boldsymbol{q}}_h \end{bmatrix} + \begin{bmatrix} \boldsymbol{K}_n + \boldsymbol{K}_b & -\boldsymbol{K}_b \\ -\boldsymbol{K}_b & \boldsymbol{K}_h + \boldsymbol{K}_b \end{bmatrix} \begin{bmatrix} \boldsymbol{q}_n \\ \boldsymbol{q}_h \end{bmatrix} = 0, \quad (28)$$

where $\boldsymbol{K}_{\mathrm{h}}$, $\boldsymbol{C}_{\mathrm{h}}$, and $\boldsymbol{M}_{\mathrm{h}}$ denote the stiffness, damping, and mass matrix of the housing bearing seat, respectively. $\boldsymbol{K}_{\mathrm{n}}$, $\boldsymbol{C}_{\mathrm{n}}$, and $\boldsymbol{M}_{\mathrm{n}}$ denote the stiffness, damping, and mass matrix of the shaft neck, respectively.

Fig. 6 shows the MGDM, where $OXYZ$ is the system generalized coordinate; its $X$-axis is parallel to input shaft 2 of the high-speed stage, the $Z$-axis coincides with carrier shaft 1, and the $Y$-axis is perpendicular to the $OXZ$ plane.

$$\boldsymbol{M}\ddot{\boldsymbol{q}} + (\boldsymbol{C}_{\mathrm{a}} + \boldsymbol{C}_{\mathrm{b}} + \boldsymbol{C}_{\mathrm{t}})\dot{\boldsymbol{q}} + (\boldsymbol{K}_{\mathrm{a}} + \boldsymbol{K}_{\mathrm{b}} + \boldsymbol{K}_{\mathrm{t}})\boldsymbol{q} = \boldsymbol{T}, \quad (29)$$

where $\boldsymbol{K}_{\mathrm{a}}$, $\boldsymbol{K}_{\mathrm{t}}$, and $\boldsymbol{K}_{\mathrm{b}}$ denote the mesh stiffness, torsional stiffness, and radial stiffness matrix of the system, respectively. $\boldsymbol{C}_{\mathrm{a}}$, $\boldsymbol{C}_{\mathrm{t}}$, and $\boldsymbol{C}_{\mathrm{b}}$ denote the mesh damping, torsional damping, and radial damping matrix of the system, respectively; $\boldsymbol{q}$ represents the generalized coordinate vector; $\boldsymbol{M}$ represents the mass matrix; and $\boldsymbol{T}$ represents the load vector.

## IV. MODEL UPDATING

This section describes the manner in which the proposed updating method was used to update the MGDM in MATLAB software. Subsequently, the simulation results before and after updating are compared with the experimental results to verify the effectiveness of the method.

### A. CONSTRUCTION AND SELECTION OF SURROGATE MODEL

In this section, the optimal Latin hypercube sampling method [26] was first used to extract the sample data uniformly. Subsequently, KRG, the RBF, and the SVM as described in Section 2.1 were used to construct the surrogate model of the MGDM. Finally, the prediction accuracy of these surrogate models was verified based on the error square, $R^2$, and the KRG with the highest accuracy was selected as the final surrogate model for subsequent Sobol sensitivity analysis and genetic updating.

Based on the vibration standard, when the excitation frequency is greater than 1000 Hz, the vibration acceleration of the gearbox should be tested. Because the excitation frequency of the multistage gearbox in this study is primarily high (≥1000 Hz) and the vibration intensity is proportional to the acceleration in the high-frequency range, the spatial vibration acceleration root mean square (SVARMS) of each measuring point was selected as the evaluation index, calculated as follows:

$$\mathrm{P}_n = \sqrt{[\sum_{i=1}^{N}(\sqrt{x_{ni}^2 + y_{ni}^2 + z_{ni}^2})^2]/N}, \tag{30}$$

where $N$ represents the number of data points; $x_{ni}$, $y_{ni}$, and $z_{ni}$ $(n = 1, 2, \ldots, 5)$ represent the vibration acceleration of measuring point $n$ along the generalized coordinate axis direction.

After determining the geometric parameters and materials, the initial values of the mesh stiffness (MS), radial bearing stiffness (RBS), and axial bearing stiffness (ABS) were obtained using the finite element method (see Table 1). In Table 1, the unit of stiffness is N/m. To ensure the physical sense of the stiffness parameters in the updating process, its updating range was set at [−3%, 3%]. As it is difficult to determine the damping parameter [24], its initial value was estimated empirically using Eq. (17). According to Yi *et al.*, [22] the range of the mesh damping ratio (MDR) is [0.03, 0.17], and the range of the bearing damping ratio (BDR) is [2e-5, 5e-3].

Training and validation samples are the basis for establishing and verifying the surrogate model. The optimal Latin hypercube sampling method [26] is an effective method for obtaining training and validation samples. The method exhibits good stability and can yield uniformly distributed sample points. Therefore, the optimal Latin hypercube sampling method was adopted in this study to extract 400 sets of training samples and 40 sets of validation samples within the value range of the updating parameters. Subsequently, each set of samples was input to the MGDM to calculate the corresponding evaluation index value (see Eq. 30).

**TABLE 1. Initial value and value range of model parameters.**

| Model parameter | Initial | Range |
|---|---|---|
| $x_1$, MS of high-speed stage | 5.7e8 | [5.55e8,5.87e8] |
| $x_2$, MDR of high-speed stage | 0.1 | [0.03,0.17] |
| $x_3$, MS of inter-speed stage | 4.8e8 | [4.65e8,4.94e8] |
| $x_4$, MDR of inter-speed stage | 0.1 | [0.03,0.17] |
| $x_5$, MS of low-speed stage | 3.7e8 | [3.58e8,3.81e8] |
| $x_6$, MDR of low-speed stage | 0.1 | [0.03,0.17] |
| $x_7$, MS of planetary stage | 9.5e8 | [9.21e8,9.78e8] |
| $x_8$, MDR of planetary stage | 0.1 | [0.03,0.17] |
| $x_9$, RBS of planet bearing | 3.4e6 | [3.29e6,3.50e6] |
| $x_{10}$, BDR of planet bearing | 1e-3 | [2e-5,5e-3] |
| $x_{11}$, Ring support stiffness | 2e9 | [1.94e9,2.06e9] |
| $x_{12}$, Ring support damping | 1e-3 | [2e-5,5e-3] |
| $x_{13}$, RBS of bearings 1 and 2 | 1.5e7 | [1.46e7,1.55e7] |
| $x_{14}$, BDR of bearings 1 and 2 | 1e-3 | [2e-5,5e-3] |
| $x_{15}$, RBS of bearings 3 and 4 | 5.1e8 | [4.94e8,5.25e8] |
| $x_{16}$, ABS of bearings 3 and 4 | 1.7e8 | [1.64e8,1.75e8] |
| $x_{17}$, BDR of bearings 3 and 4 | 1e-3 | [2e-5,5e-3] |
| $x_{18}$, RBS of bearings 5 and 6 | 4.1e8 | [3.97e8,4.22e8] |
| $x_{19}$, ABS of bearings 6 and 6 | 3.4e8 | [3.29e8,3.50e8] |
| $x_{20}$, BDR of bearings 5 and 6 | 1e-3 | [2e-5,5e-3] |
| $x_{21}$, RBS of bearings 7 and 8 | 5.5e8 | [5.33e8,5.66e8] |
| $x_{22}$, ABS of bearings 7 and 8 | 6.2e8 | [6.01e8,6.38e8] |
| $x_{23}$, BDR of bearings 7 and 8 | 1e-3 | [2e-5,5e-3] |
| $x_{24}$, RBS of bearings 9 and 10 | 4.2e8 | [4.07e8,4.32e8] |
| $x_{25}$, ABS of bearings 9 and 10 | 2.0e8 | [1.94e8,2.06e8] |
| $x_{26}$,BDR of bearings 9 and 10 | 1e-3 | [2e-5,5e-3] |

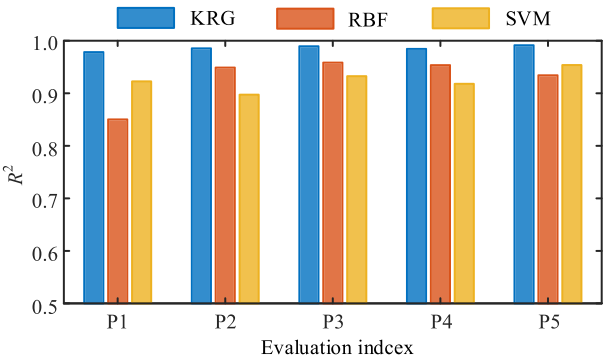


**FIGURE 7. Prediction accuracy comparison of evaluation indicators P1–P5 of three surrogate models.**

To eliminate the order of magnitude difference and ensure the accuracy of the surrogate model, the min–max method was used to normalize the sample data, expressed as follows:

$$x_k = (x_k - x_{\min})/(x_{\max} - x_{\min}) \tag{31}$$

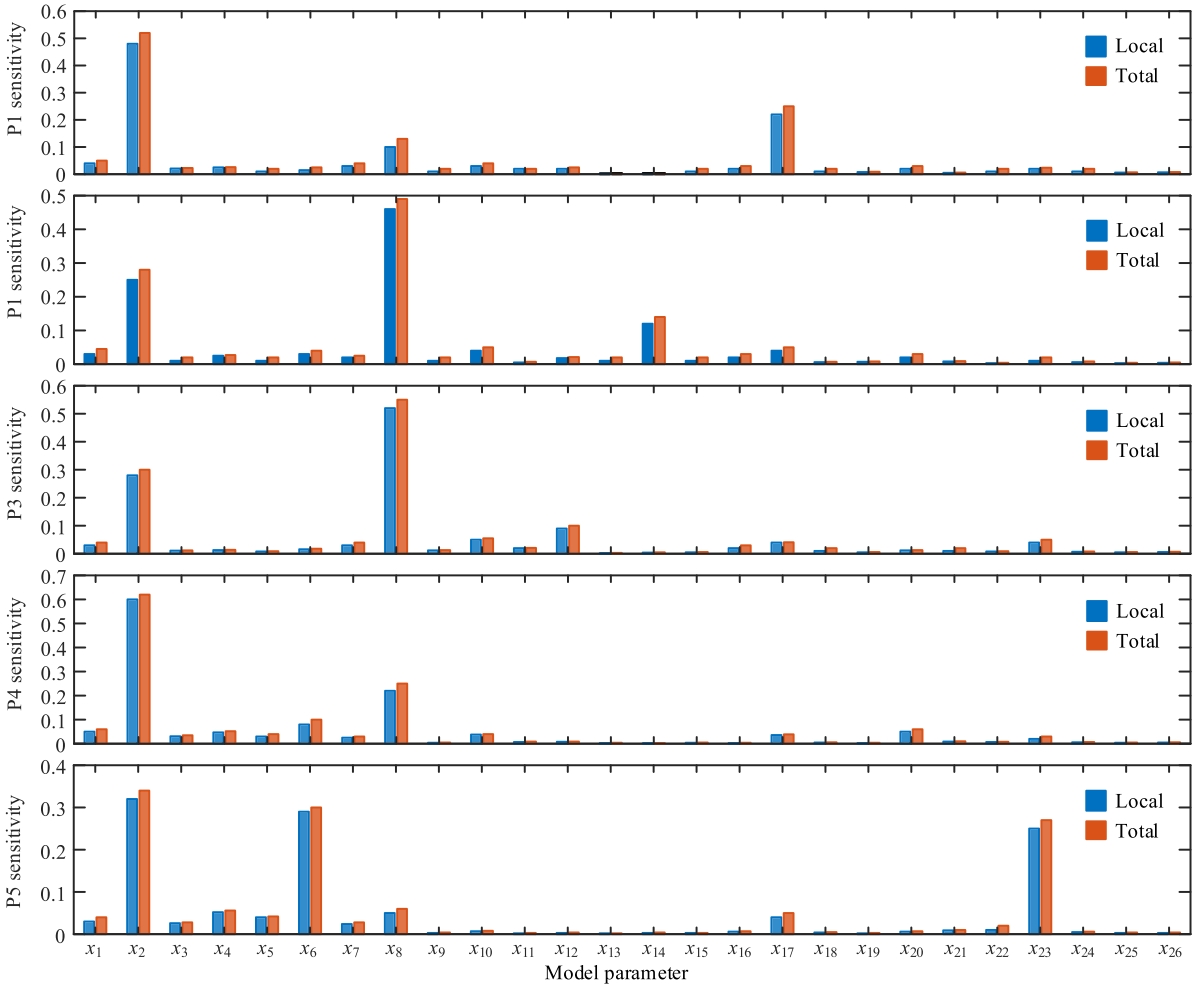


**FIGURE 8.** Sensitivity of 26 model parameters to five evaluation indexes P1–P5 in MGDM.

where $x_{\min}$ and $x_{\max}$ denote the minimum and maximum numbers in the sample data column vector, respectively.

Next, the KRG, the RBF, and the SVM were adopted to establish the surrogate model of the MGDM. Subsequently, $R^2$ (see Eq. 32) was used to quantify the prediction accuracy of these surrogate models to select the surrogate model with the highest accuracy.

$$R^2 = 1 - \sum_{j=1}^{m} (P_j - \hat{P}_j)^2 \sum_{j=1}^{m} (P_j - \bar{P}_j)^2, \tag{32}$$

where $m$ represents the number of validation samples, $P_j$ represents the actual value obtained from the MGDM, $P_j$ represents the predicted value obtained from the surrogate model, and $\bar{P}_j$ represents the mean value of the actual value.

In Fig. 7, an $R^2$ value closer to 1 indicates a higher prediction accuracy of the surrogate model. Compared with prediction accuracies of the RBF and SVM, that of KRG was higher (see Fig. 7), and the $R^2$ of its five evaluation indexes, P1–P5, were greater than 0.97. This indicates that KRG is the most suitable surrogate model to replace the MGDM.

In summary, among the KRG, RBF, and SVM surrogate models established in this section, the prediction accuracy of KRG was the highest, rendering it suitable for effectively replacing the time-consuming MGDM. Therefore, KRG was used as the final surrogate model for subsequent Sobol sensitivity analysis and genetic updating.

### B. UPDATING PARAMETER SCREENING BASED ON SOBOL SENSITIVITY ANALYSIS

To screen the updating parameters and improve the calculation efficiency, the selected KRG surrogate model was combined with the Sobol method to analyze the parameter sensitivity of the MGDM.

In Sobol sensitivity analysis, the local sensitivity reflects the effect of individual parameters on the system output. The global sensitivity not only reflects the effect of individual parameters but also reflects the effects of a parameter acting simultaneously with other parameters on the system output. Fig. 8 shows the local and global sensitivities of the 26 model parameters to five evaluation indexes P$n$ ($n = 1, 2, \ldots, 5$) in the MGDM. As shown in Fig. 8, seven parameters exhibited

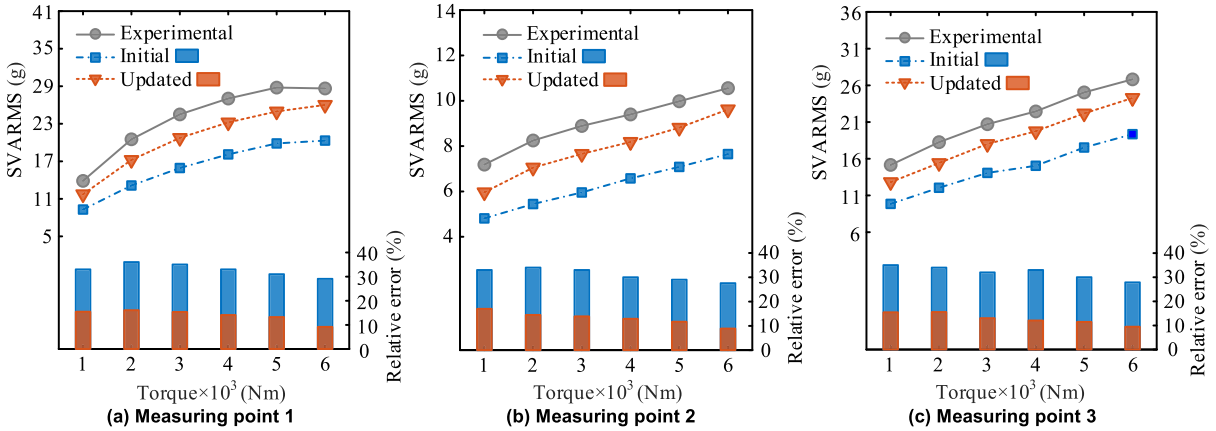


**FIGURE 9.** Comparison of simulation and experimental results from MGDM before and after updating under different torques.

greater sensitivity among the 26 parameters, i.e., $x_2$, $x_6$, $x_8$, $x_{12}$, $x_{14}$, $x_{17}$, and $x_{23}$.

In conclusion, the sensitivity analysis method can be used to screen the updating parameters from the numerous parameters of the MGDM, thereby providing a foundation for the subsequent model updating.

### C. MODEL UPDATING BASED ON GENETIC ALGORITHM

To improve the calculation efficiency, the KRG surrogate model was combined with the genetic algorithm [27]–[29] to determine parameter values that minimize the error between the simulation and experimental results within the value range of the updating parameters to improve the accuracy of the MGDM.

The goal of model updating is to minimize the error between the simulation and experimental results by constantly adjusting the updating parameters. Therefore, the updating objective $F(\boldsymbol{x})$ can be defined as

$$\begin{cases} \min F(\boldsymbol{x}) = \dfrac{1}{5}\displaystyle\sum_{n=1}^{5}\left|\dfrac{P_n^{test} - P_n^{model}}{P_n^{test}}\right|, \\ s.t \ \ (\boldsymbol{x})^{LB} \le (\boldsymbol{x}) \le (\boldsymbol{x})^{LB} \end{cases} \tag{33}$$

where $\boldsymbol{x}$ represents the updating parameter vector, $\boldsymbol{x} = [x_2, x_6, x_8, x_{12}, x_{14}, x_{17}, x_{23}]$; $\boldsymbol{x}^{\mathrm{LB}}$ and $\boldsymbol{x}^{\mathrm{UB}}$ denote the upper and lower limits of the updating parameters, respectively; $P_n^{test}$ and $P_n^{model}$ denote the experimental and simulation evaluation index values of the $n$th measuring point, respectively; $P_n^{model}$ is provided by the KRG surrogate model; and $P_n^{test}$ is based directly on the experimental results.

After establishing the updating objective, the genetic algorithm was used to search the optimal parameter values across the entire value range of the updating parameters to minimize the updating objective. In the updating process, the population size was 100, and the evolutionary algebra was 150. The initial and updated values of the updating parameters are shown in Table 2. The updating rate $\zeta$ of the model parameters is expressed as $\zeta = |(x\text{-}x_0)/x_0|$; where $x_0$ and $x$ denote the initial and updated values of the updating parameters, respectively. As shown in Table 2, the damping parameters changed significantly before and after updating. This is because the damping initial value was difficult to determine and the value range was large, not because the geometric parameters and material properties have changed. In other words, the most suitable damping parameter values were obtained through model updating, which improved the accuracy of the calculation results of the MGDM.

**TABLE 2.** Initial and updated value of updating parameters.

| Parameter | Initial | Updated | $\zeta$(%) |
|---|---|---|---|
| $x_2$ | 1e-1 | 3.25e-2 | 67.50 |
| $x_6$ | 1e-1 | 4.18e-2 | 58.20 |
| $x_8$ | 1e-1 | 3.94e-2 | 60.60 |
| $x_{12}$ | 1e-3 | 2.52e-5 | 97.48 |
| $x_{14}$ | 1e-3 | 3.41e-5 | 96.59 |
| $x_{17}$ | 1e-3 | 6.79e-5 | 93.21 |
| $x_{23}$ | 1e-3 | 4.37e-5 | 95.63 |

The accuracy of the MGDM was evaluated by calculating the relative error between the simulation and experimental evaluation indexes, as follows:

$$E_n = \frac{P_n^{test} - P_n^{model}}{P_n^{test}} \times 100\% \tag{34}$$

The initial and updated values of the updating parameters in Table 2 were input to the MGDM to calculate the simulation results of five evaluation indexes before and after updating; subsequently, the results were compared with the experimental results (see Table 3). As shown in Table 3, compared with the initial model, the updated MGDM can predict the dynamic characteristics of the actual system more accurately, and the model accuracy improved significantly. This indicates that the proposed updating method can significantly improve the accuracy of the MGDM under a specific torque; however, further investigations are required to

**TABLE 3. Comparison of simulation and experimental results from MGDM before and after updating at 6000 Nm torque.**

| Evaluation index | Experimental (g) | Dynamic model (g) | | Relative error (%) | | |
|---|---|---|---|---|---|---|
| | | Initial | Updated | Initial | Updated | Improvement ratio |
| $P_1$ | 28.65 | 20.32 | 26.02 | 29.07 | 9.17 | 19.89 |
| $P_2$ | 10.56 | 7.65 | 9.62 | 27.55 | 8.86 | 18.68 |
| $P_3$ | 26.82 | 19.35 | 24.28 | 27.84 | 9.47 | 18.37 |
| $P_4$ | 20.78 | 14.77 | 18.97 | 28.91 | 8.74 | 20.17 |
| $P_5$ | 14.76 | 10.66 | 13.35 | 27.80 | 9.53 | 18.27 |
| Average value | | | | 28.24 | 9.15 | 19.09 |

confirm whether the model accuracy can also be improved under other torques.

A comparison of the simulation and experimental results before and after updating under different torques of 1000–6000 Nm is shown in Fig. 9. As shown, the vibration of the multistage gearbox increased with the torque. Compared with the initial model, the accuracy of the updated MGDM improved significantly. This verifies that the proposed updating method can effectively improve the accuracy of the calculation results of the MGDM; as such, the updated MGDM can be applied more accurately to the subsequent dynamic design.

In conclusion, the proposed updating method can significantly improve the accuracy of the MGDM, and the updated MGDM can more accurately predict the dynamic characteristics of the actual system, thereby providing an effective analysis model for the subsequent dynamic design.

## V. CONCLUSION

Time-consuming calculations and numerous parameters render it difficult to update the MGDM using previous updating methods. Therefore, an improved updating method suitable for the MGDM based on a surrogate model and sensitivity analysis was proposed. The purpose of using the surrogate model is to solve the problem of low computational efficiency by replacing the time-consuming MGDM. The function of the sensitivity analysis is to screen effective updating parameters from numerous parameters. Subsequently, the genetic algorithm is used to search for the most suitable parameters within the value range of the updating parameters, such that the simulation result is similar to the experimental result. The results showed that the improved updating method proposed herein can effectively improve the accuracy of the calculation results of the MGDM. The accuracy of the calculation results of the updated MGDM improved significantly compared with that of the initial model, thereby providing a more accurate prediction of the dynamic characteristics of the actual system as well as an effective analytical model for the dynamic design of the multistage gearbox in the subsequent step.

## REFERENCES

[1] S. Wang, A. Xieeryazidan, X. Zhang, and J. Zhou, "An improved computational method for vibration response and radiation noise analysis of two-stage gearbox," *IEEE Access*, vol. 8, pp. 85973–85988, 2020.
[2] Y. Zhao, Y. Liu, X. Xin, S. Yu, H. Ma, and Q. Han, "Dynamic modelling considering nonlinear factors of coupled spur gear system and its experimental research," *IEEE Access*, vol. 8, pp. 84971–84980, 2020.
[3] M. Shuai, M. Shuai, J. G. Guang, and Y. Z. Xiang, "Research on dynamic load-sharing characteristics of two-stage asymmetric star gear system," *IEEE Access*, vol. 7, pp. 126799–126811, 2019.
[4] M. Cuadrado, J. A. Artero-Guerrero, J. Pernas-Sánchez, and D. Varas, "Model updating of uncertain parameters of carbon/epoxy composite plates from experimental modal data," *J. Sound Vibrat.*, vol. 455, pp. 380–401, Sep. 2019.
[5] J. Jang and A. W. Smyth, "Model updating of a full-scale FE model with nonlinear constraint equations and sensitivity-based cluster analysis for updating parameters," *Mech. Syst. Signal Process.*, vol. 83, pp. 337–355, Jan. 2017.
[6] X. Zhai, C.-W. Fei, Y.-S. Choy, and J.-J. Wang, "A stochastic model updating strategy-based improved response surface model and advanced Monte Carlo simulation," *Mech. Syst. Signal Process.*, vol. 82, pp. 323–338, Jan. 2017.
[7] Z. Deng, Z. Guo, and X. Zhang, "Interval model updating using perturbation method and radial basis function neural networks," *Mech. Syst. Signal Process.*, vol. 84, pp. 699–716, Feb. 2017.
[8] G. Sun, M. Deng, G. Zheng, and Q. Li, "Design for cost performance of crashworthy structures made of high strength steel," *Thin-Walled Struct.*, vol. 138, pp. 458–472, May 2019.
[9] S. Zhou, C. Li, Y. Xiao, and P. W. Cheng, "Importance of platform mounting orientation of Y-shaped semi-submersible floating wind turbines: A case study by using surrogate models," *Renew. Energy*, vol. 156, pp. 260–278, Aug. 2020.
[10] H. Sarmadi, A. Karamodin, and A. Entezami, "A new iterative model updating technique based on least squares minimal residual method using measured modal data," *Appl. Math. Model.*, vol. 40, nos. 23–24, pp. 10323–10341, Dec. 2016.
[11] N. Guo, Z. Yang, L. Wang, Y. Ouyang, and X. Zhang, "Dynamic model updating based on strain mode shape and natural frequency using hybrid pattern search technique," *J. Sound Vibrat.*, vol. 422, pp. 112–130, May 2018.
[12] Q. Shao, E. Gao, T. Mara, H. Hu, T. Liu, and A. Makradi, "Global sensitivity analysis of solid oxide fuel cells with Bayesian sparse polynomial chaos expansions," *Appl. Energ.*, vol. 260, pp. 1–14, Feb. 2020.
[13] A. Pietrenko-Dabrowska, S. Koziel, and M. Al-Hasan, "Cost-efficient bi-layer modeling of antenna input characteristics using gradient kriging surrogates," *IEEE Access*, vol. 8, pp. 140831–140839, 2020.
[14] T. Houret, P. Besnier, S. Vauchamp, and P. Pouliguen, "Controlled stratification based on kriging surrogate model: An algorithm for determining extreme quantiles in electromagnetic compatibility risk analysis," *IEEE Access*, vol. 8, pp. 3837–3847, 2020.
[15] Z. Tang, M. Wang, Y. Hu, Z. Mei, J. Sun, and L. Yan, "Optimal design of traction gear modification of high-speed EMU based on radial basis function neural network," *IEEE Access*, vol. 8, pp. 134619–134629, 2020.
[16] M. Amirian and F. Schwenker, "Radial basis function networks for convolutional neural networks to learn similarity distance metric and improve interpretability," *IEEE Access*, vol. 8, pp. 123087–123097, 2020.
[17] H. Jie, G. Zheng, J. Zou, X. Xin, and L. Guo, "Adaptive decoupling control using radial basis function neural network for permanent magnet synchronous motor considering uncertain and time-varying parameters," *IEEE Access*, vol. 8, pp. 112323–112332, 2020.

[18] R. E. Caraka, Y. Lee, R.-C. Chen, and T. Toharudin, "Using hierarchical likelihood towards support vector machine: Theory and its application," *IEEE Access*, vol. 8, pp. 194795–194807, 2020.
[19] J. Li, M. Ye, W. Meng, X. Xu, and S. Jiao, "A novel state of charge approach of lithium ion battery using least squares support vector machine," *IEEE Access*, vol. 8, pp. 195398–195410, 2020.
[20] X. Ren, Y. Wang, T. Guo, and Q. Wang, "Robust adaptive beamforming using support vector machines," *IEEE Access*, vol. 8, pp. 137955–137965, 2020.
[21] A. Saltelli and I. M. Sobol', "Sensitivity analysis for nonlinear mathematical models: Numerical experience," *Matematicheskoe Modelirovanie*, vol. 7, pp. 16–28, 1993.
[22] Y. Yi, D. Qin, and C. Liu, "Investigation of electromechanical coupling vibration characteristics of an electric drive multistage gear system," *Mechanism Mach. Theory*, vol. 121, pp. 446–459, Mar. 2018.
[23] H. Xu, D. Qin, C. Liu, Y. Yi, and H. Jia, "Dynamic modeling of multistage gearbox and analysis method of resonance danger path," *IEEE Access*, vol. 7, pp. 154796–154807, 2019.
[24] M. Kubur, A. Kahraman, D. M. Zini, and K. Kienzle, "Dynamic analysis of a multi-shaft helical gear transmission by finite elements: Model and experiment," *J. Vibrat. Acoust.*, vol. 126, no. 3, pp. 398–406, Jul. 2004.
[25] S. Wang, Y. Shen, and H. Dong, "Nonlinear dynamical characteristics of a spiral bevel gear system with backlash and time-varying stiffness," *Chin. J. Mech. Eng.*, vol. 39, no. 2, pp. 28–32, 2003.
[26] X. He, W. Gou, Y. Liu, and Z. Gao, "Structure and system nonprobabilistic reliability solution method based on enhanced optimal latin hypercube sampling," *Int. J. Struct. Stability Dyn.*, vol. 15, no. 1, pp. 1–16, 2015.
[27] A. B. Ibrahim, Y. M. Seddiq, A. H. Meftah, M. Alghamdi, S.-A. Selouani, M. A. Qamhan, Y. A. Alotaibi, and S. A. Alshebeili, "Optimizing arabic speech distinctive phonetic features and phoneme recognition using genetic algorithm," *IEEE Access*, vol. 8, pp. 200395–200411, 2020.
[28] Y. Jin and B. Ko, "Restoring latent vectors from generative adversarial networks using genetic algorithms," *IEEE Access*, vol. 8, pp. 199673–199681, 2020.
[29] P. W. Khan and Y.-C. Byun, "Genetic algorithm based optimized feature engineering and hybrid machine learning for effective energy consumption prediction," *IEEE Access*, vol. 8, pp. 196274–196286, 2020.

**HUACHAO XU** was born in Xinjiang, China, in 1990. He is currently pursuing the Ph.D. degree with Chongqing University, China. Since 2013, he has been working on dynamic modeling and vibration reduction of gearboxes. His current research interests include the dynamic modeling, dynamic model updating, and vibration analysis of gearbox.

**DATONG QIN** was born in Chongqing, China, in 1956. He received the Ph.D. degree from Chongqing University, Chongqing, and from Tohoku University, Ishinomaki, Japan, in 1993. He currently works with Chongqing University. Meanwhile, he is also a Full Professor, the Deputy Director of Academic Committee with the State Key Laboratory of Mechanical Transmission, and the Director of Power Transmission Institute. His current research interests include mechanical transmission, power transmission, and comprehensive control of vehicles.

**CHANGZHAO LIU** received the Ph.D. degree from the Department of Mechanical Engineering, Chongqing University, China, in 2016. He is currently a Lecturer with Chongqing University. His current research interests include integrated design and analysis of electromechanical transmission system for new energy vehicles.

**YANG ZHANG** was born in Shandong, China, in 1997. She is currently pursuing the master's degree with the Dalian University of Technology, China. Her current research interests include the optimization design and application of surrogate models based on adaptive sequential sampling methods.